Data-driven framework for the prediction of PEGDA hydrogel mechanics

Yongkui Tang[1,2], Michal Levin[3], Olivia G. Long[2,4], Claus D. Eisenbach[2,5], Noy Cohen[3], and Megan T. Valentine[1,2,*]

[1]Department of Mechanical Engineering, University of California, Santa Barbara, CA 93106, USA
[2]Materials Research Laboratory, University of California, Santa Barbara, CA 93106, USA
[3]Department of Materials Science and Engineering, Technion - Israel Institute of Technology, Haifa 3200003, Israel
[4]Materials Department, University of California, Santa Barbara, CA 93106, USA
[5]Institut für Polymerchemie, University of Stuttgart, Stuttgart D-70569, Germany
[*]Corresponding Author: valentine@engineering.ucsb.edu

November 19, 2024

Abstract

Poly(ethylene glycol) diacrylate (PEGDA) hydrogels are biocompatible and photocrosslinkable, with accessible values of elastic modulus ranging from kPa to MPa, leading to their wide use in biomedical and soft materials applications. However, PEGDA gels possess complex microstructures, limiting the use of standard polymer theories to describe them. As a result, we lack a foundational understanding of how to relate their composition, processing, and mechanical properties. To address this need, we use a data-driven approach to develop an empirical predictive framework based on high-quality data obtained from uniaxial compression tests and validated using prior data found in the literature. The developed framework accurately predicts the hydrogel shear modulus and a strain-stiffening coefficient using only synthesis parameters, such as the molecular weight and initial concentration of PEGDA, as inputs. These results provide simple and reliable experimental guidelines for precisely controlling both the low-strain and high-strain mechanical responses of PEGDA hydrogels, thereby facilitating their design for various applications.

Keywords: design, modeling, characterization, strain-stiffening, crosslinked, bottlebrush

Introduction

Poly(ethylene glycol) diacrylate (PEGDA) hydrogels have found extensive use in biomedical applications, including tissue engineering,[1–4] drug delivery,[5–7] traction force microscopy,[8,9] and microfluidics[10,11] due to their biocompatibility, mechanical tunability, low cost, and ability to be functionalized with biomolecules such as peptides and growth factors.[3,4] Moreover, PEGDA-based materials are easily photopolymerized and photocrosslinked.[1–11] This enables the facile and high-resolution fabrication of intricate structures with tailored mechanical properties and makes PEGDA an attractive choice for many soft material applications.[2,5]

However, despite the wide use of PEGDA hydrogels, our ability to accurately predict their mechanical properties remains limited. Models based on classical theories[12–14] work well for homogeneous networks such as tetra-PEG gels.[15] Unfortunately, these models often fail to provide an accurate prediction for PEGDA hydrogels due to the heterogeneity of their network structures.[16] Most ideal polymer networks are imagined as long polymer chains that are physically or covalently crosslinked by point-like junctions (Fig. 1a). By contrast, bifunctional PEGDA acts as both macromonomer and crosslinker during polymerization. Thus, the resulting network is characterized by interpenetrating bottlebrushes consisting of polyacrylate (PA) backbones with PEG side chains which simultaneously act as crosslinking chains between adjacent PA chains (Fig. 1b). This structure has been deduced from X-ray scattering experiments of PEGDA hydrogels that report the formation of highly branched star polymers with PEG chains connecting PA cores[16] or as molecular bottlebrushes with a PA backbone decorated with PEG side chains.[17] Other studies have confirmed the presence of extended PA backbones with degrees of polymerization on the order of 100 or more when monofunctional PEG-acrylate macromonomers are copolymerized with PEGDA.[18,19] While we expect that the PEG chains in crosslinked PEG hydrogels should be elastically active for any network preparation method, the presence of the stiff polyacrylate chain in PEGDA gels forms a distinct reinforcing, backbone structure within the PEGDA hydrogels. These features also limit the applicability of more recent

frameworks for hydrogel design, which cannot account for interpenetrating networks, or for networks formed from more than one polymer type or those having non-linear architectures or extended junctions.[20–22]

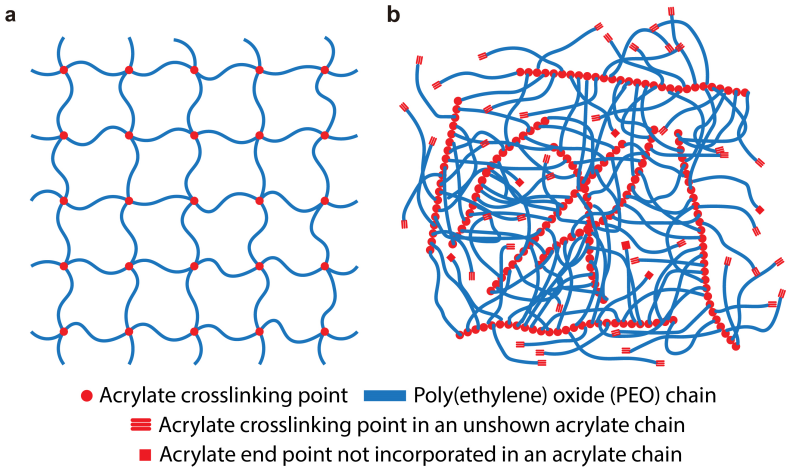

Figure 1: Two-dimensional schematic diagrams illustrating different hydrogel network structures. (a) Part of a homogeneous ideal network with point-like crosslinking junctions (red) and crosslinked chains (blue). For simplicity, only portions of the boundary blue chains are shown, which are parts of longer chains connected to red crosslinking points (not shown); (b) Part of a PEGDA hydrogel network consisting of randomly oriented interpenetrating bottlebrushes with rod-like polyacrylate core (red) and random-coil PEG crosslinking chains (blue), inferred from scattering experiments.[16,17]

There are other limitations in predicting the mechanical properties of PEGDA hydrogels. For example, in order to calculate the shear modulus, existing models require the polymer volume fraction in the equilibrium swollen state (ϕ) as an input parameter. Although equilibrium swelling theory offers a method to calculate this quantity based on synthesis parameters for ideal networks,[14,23,24] the results often deviate significantly from the measurement of PEGDA gels (Fig. S16). As a result, ϕ must be determined experimentally using hydrogels that have been synthesized and fully swollen, limiting the use of theory in material design. Other studies have used data-driven approaches to develop empirical relationships between different measures of network swelling, microstructure and mechanics, but these have not connected the model outputs to synthesis parameters, limiting their use in network

design.[16,25–27] We recently developed a microstructurally motivated model that captures the essential features that enable deformation in PEGDA hydrogels including the entropic elasticity of PEG chains and the deformation of the stiff PA rods, as well as the PA–PA interactions.[28] This model captures the microstructural evolution of the network during loading and reveals the role of key microscopic quantities. However, to provide useful predictions at the material design stage, the model requires an understanding of how the synthesis parameters relate to the molecular weight distribution of the PA chains, a quantity that is very challenging to access experimentally. Thus, despite progress in the development of models of hydrogel networks, in practice, the mechanical design of PEGDA hydrogels usually requires an inefficient and labor-intensive trial-and-error process.[20]

To better understand the mechanical properties of PEGDA hydrogels and to provide a reliable design guideline for their use, we developed a data-driven framework for predicting the shear modulus and strain-stiffening coefficient based solely on known synthesis parameters. We systematically studied 35 distinct formulations of PEGDA hydrogels, with number-averaged molecular weights ranging from approximately 0.5 to 6 kDa and over a wide range of initial PEGDA concentrations. To ensure reproducibility and high data quality, hydrogel disks were fabricated via a high-precision replica molding method. Using experimentally determined data from uniaxial compression tests, we established an empirical relationship between the shear modulus and PEGDA concentration and molecular weight, which is based on classical theory[12,29,30] but modified to capture the influence of the structural complexity of the PEGDA hydrogels. Additionally, we developed a simple relationship between the strain-stiffening coefficient and the PEGDA molecular weight. Our predictive model, which is validated through a comprehensive comparison to previously published data on similar materials, accurately captures the linear elastic responses of PEGDA hydrogels, as well as the high-strain response to compression. Importantly, our approach allows this estimation to be made at the design stage thus minimizing the need for pilot testing and trial-and-error experimentation and accelerating material analysis and optimization for specific applications.

Materials and Methods

Materials

PEGDA starting materials of nominal number-averaged molecular weight M_n ranging between 0.5 kDa and 6.0 kDa were purchased through commercial sources (0.5 kDa from TCI America, 0.7 kDa from Millipore Sigma, 1.0 kDa from Polysciences, 3.4 kDa from Thermo Fisher Scientific, and 2.0 kDa and 6.0 kDa from Biopharma PEG Scientific).

The remaining reagents were sourced as follows. The photoinitiator lithium phenyl(2,4,6-trimethylbenzoyl) phosphinate (LAP) was obtained from TCI America. Glass coverslips (Corning #1 22 x 40 mm^2) were purchased from ThermoFisher Scientific. Polydimethylsiloxane (PDMS) (Sylgard 184, Dow Corning) was purchased from Krayden. 5 cSt silicone oil (trimethylsiloxy-terminated polydimethylsiloxane, DMS-T05) was purchased from Gelest. Glass microscope slides were purchased from VWR International. Deionized (DI) water was purified by an in-house Milli-Q Advantage A10 water purification system.

Hydrogel Fabrication

The fabrication process is illustrated in Fig. 2. To ensure good measurement reproducibility, hydrogel disks with high geometric uniformity were fabricated via a high-precision replica molding method using PDMS molds with circular through-holes (Fig. 2a). The PDMS molds were also fabricated by replica molding, as described in Supplementary Information §3. For each of 35 formulations, eight hydrogel disks with as-prepared diameters and heights of 6 and 3 mm, respectively, were made (Fig. 2b).

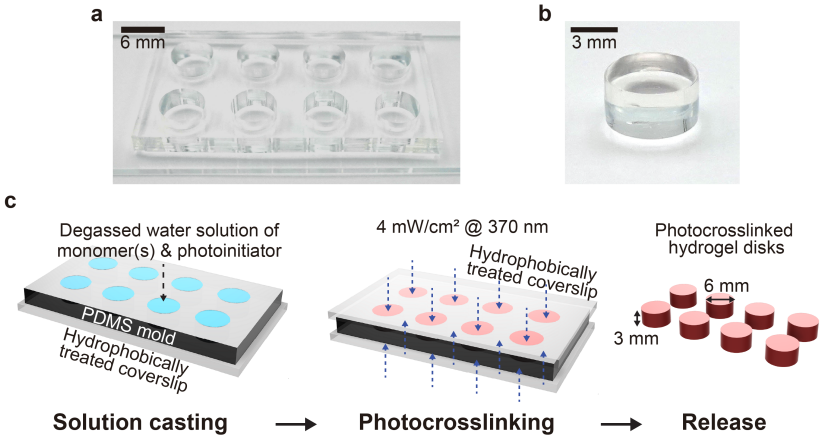

Figure 2: Schematic diagrams and photos showing the hydrogel fabrication process and fabricated hydrogels: Photos of (a) a PDMS mold with eight circular through-holes and (b) a fabricated hydrogel disk. (c) Schematic diagrams of the hydrogel disk fabrication process.

To create the hydrogel disks, an aqueous precursor solution of PEGDA macromonomers and 4.95 mM LAP was prepared. Several steps were taken to reduce the likelihood of oxygen-mediated inhibition of photopolymerization.[31] For at least 24 h prior to hydrogel fabrication, the PDMS mold was stored under vacuum to remove absorbed oxygen. Prior to filling, the PDMS mold was attached to a coverslip that was hydrophobically treated to prevent adhesion to the hydrogels (Supplementary Information §4). The precursor solution was degassed by purging with argon gas for 1 min per 1 mL solution and was immediately cast into the openings of the PDMS mold (Fig. 2c). The top side of the mold was then sealed with another hydrophobically treated coverslip. Throughout the fabrication process, the PDMS mold was placed in a custom-made argon-purging chamber that accommodates two PDMS molds, allowing the fabrication of sixteen hydrogel disks per batch (Fig. S2c and S2d).

Photopolymerization was performed by placing the filled mold within the argon-purging chamber under an ultraviolet (UV) lamp (UVP UVL-28 EL, Analytik Jena) (Fig. S2d) that provides uniform light intensity with an irradiance of 4.0 mW/cm^2 measured at 370 nm, the local absorption maximum of LAP.[32] To ensure complete crosslinking across the full disk thickness (as verified by the low sol

fraction values in Table S2), each side of the mold was irradiated for 5 min. After UV exposure, the hydrogels were carefully released from the mold. The PDMS molds were then cleaned by two rounds of sonication in IPA and DI water for 15 min each and stored for repeated use.

After fabrication, the hydrogels were stored in DI water for at least seven days with the water changed every other day to allow them to swell to equilibrium without constraint. During this time, the polymer volume fraction in the equilibrium swollen state ϕ and sol fraction were measured by tracking the dried and swollen weights of the samples (Supplementary Information §5). The diameter and height of each swollen cylindrical hydrogel were measured using the positioning stage and normal force sensor of a texture analyzer (TA.XT Plus Connect, Stable Micro Systems) (Supplementary Information §6.)

Mechanical Characterization and Data Analysis

Uniaxial compression tests were performed on fully swollen samples using the texture analyzer with a 50-mm-diameter metal plate fixture and 55-N load cell. Before each test, 4 μL of 5 cSt silicone oil, which acted as a lubricant, was applied to the top and bottom surfaces of the hydrogel, as well as the metal fixture and a glass microscope slide upon which the hydrogel was placed. No obvious sidewall barreling was observed under any condition, suggesting that the surfaces are sufficiently lubricated to achieve minimal friction (Fig. S7). For each formulation, four samples were tested. During each test, the hydrogel specimen was compressed quasistatically at a rate of 0.01 mm/s to minimize the influence of strain rate on the response until the specimen ruptured or the force limit of the load cell was reached during which the force and displacement data were recorded (Supplementary Information Video S1). Control measurements were performed without lubrication in order to assess whether water was exuded during compression, and no water was observed, suggesting that poroelastic effects were small and could be neglected. Additionally, the non-lubricated gels were weighed before and after compression and the weight loss was $< 3\%$, which we regard as negligible.

Due to the presence of the lubricant and because the hydrogel surface was not perfectly flat, we

observed that the measured force started to increase before proper contact between the sample and the compression fixture was achieved. To identify the contact point, we extrapolated the linear (elastic) region of the force-displacement curve to zero force, and identified the position at this force value as the point of contact (Supplementary Information §7 and Fig. S3). To calculate the compressive engineering stress σ, the force values were normalized by the initial hydrogel area. The displacement was converted to stretch ratio λ, defined here as the ratio between the compressed height and the initial height of the sample based on the contact point position and measured hydrogel height.

All data processing was performed using MATLAB. The functions "nlinfit" and "fit" were used for nonlinear and linear regressions, respectively. Weighted fitting was used for data with error bars, with the inverse of variance assigned as the fitting weight .

Results

Extraction of Mechanical Parameters from Uniaxial Compression Tests

In each experiment, a fully-swollen cylindrical hydrogel sample was quasistatically compressed either until rupture or until the force limit of the load cell was reached, and the engineering stress as a function of stretch was determined (Fig. 3 and Supplementary Information Video S1). At small compressive strains (i.e. $\lambda \approx 1$), the material behaves elastically, leading to a linear response regime. As the compression magnitude increases, the stretch value decreases, and a nonlinear elastic response emerges. To capture the constitutive response of PEGDA hydrogels, we consider the Yeoh hyperelastic model for incompressible materials under uniaxial loading.[33] Taking the first two terms of the model yields

$$\sigma = G\left(1 + \alpha\left(\lambda^2 + \frac{2}{\lambda} - 3\right)\right)\left(\lambda - \frac{1}{\lambda^2}\right), \tag{1}$$

where σ is the engineering stress (in all stress-stretch plots, the compressive engineering stress is plotted, which is $-\sigma$), G is the shear modulus and α is a strain-stiffening coefficient. The Yeoh model allows for a wider range of strains to be captured as compared to the well-known neo-Hookean

model, while introducing only one additional fitting parameter. Note that setting $\alpha = 0$ in Equation 1 recovers neo-Hookean behavior under uniaxial loading.[34] As shown in Fig. 3, the neo-Hookean model fails to capture the strain-stiffening response at high strains, while the Yeoh model provides an accurate fit, highlighting its validity.

The fact that the full nonlinear mechanical response can be captured using only two parameters, G and α, with the simple Yeoh model is enabling. In principle, appropriate estimation of these parameters for a given PEGDA formulation can provide a good prediction of the mechanical response under compression. In this work, to guide the design of PEGDA hydrogels, we first experimentally determined the G and α values of 35 different formulations of PEGDA hydrogels by fitting their compression responses to the Yeoh model (Table S2), then we developed a data-driven framework that allows accurate estimation of G and α based solely on the synthesis parameter values that are known prior to hydrogel fabrication and characterization, with details described in the following subsections.

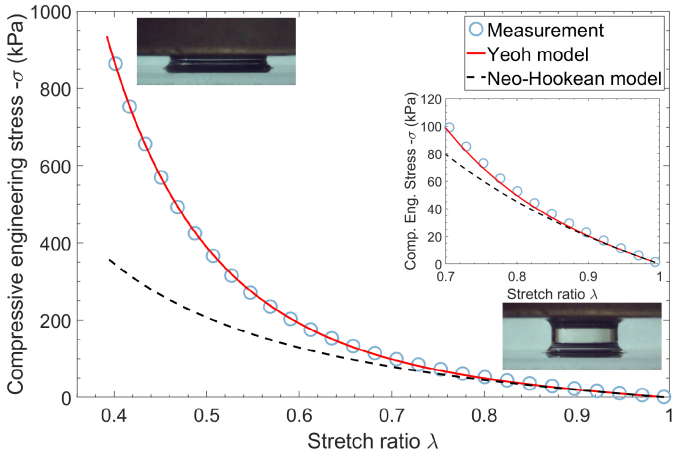

Figure 3: A measured stress vs. stretch ratio curve (symbols) and fitted curves based on the neo-Hookean (dashed black line) and Yeoh models (solid red line), respectively, along with side-view photos of a sample under compression (taken from Fig. S7). The inset shows a zoomed-in view of the curves in the low-strain (high-stretch) region. Note that only a fraction of the measured datapoints are displayed for ease of visualization; the number of fitted experimental datapoints typically exceeds 1000.

Assessment of PEGDA Properties and Formulations

To collect sufficient training data for establishing the predictive framework, we studied 35 distinct formulations of PEGDA hydrogels, wherein two easily measurable parameters, the number-averaged PEGDA molecular weight M_n and the weight/volume PEGDA concentration in the preparation state c_0, were varied over a wide range (Fig. 4 and Table S2). All other synthesis and processing parameters were held constant.

The nominal M_n of purchased PEGDA macromonomers varied from 0.5 to 6.0 kDa. From our in-house assessment based on gel permeation chromatography (GPC) (Fig. S1 and Table S1), for PEGDA macromonomers with a specified M_n of 0.5, 0.7, 1.0, and 3.4 kDa, the measured M_n values were 0.55, 0.65, 1.07, and 3.37 kDa, respectively, matching closely with manufacturers' specifications. The measured polydispersity index (PDI) values for these samples were less than 1.06. In two other cases, higher PDI values were measured. For PEGDA 2.0 kDa, the PDI was 1.67 due to a bimodal molecular weight distribution containing 1.74 kDa and 5.36 kDa components (Fig. S1d and Table S1), whereas a PDI of 1.44 was measured for PEGDA 6.0 kDa due to low- and high-molecular-weight components whose combined mol% is less than 24.0% (Fig. S1f and Table S1). Despite the higher PDI values, we deemed their quality to be acceptable for this study as the measured M_n (2.03 and 5.85 kDa) were close to the nominal values. Details of the GPC measurements are summarized in the Supplementary Information §1. In other purchased PEGDA samples, which are not reported here, we identified even more severe quality issues including incorrect molecular weight, high PDI, and multimodal molecular weight distributions. Regettably, these quality issues limited the number of commercially available PEGDA materials could be included in this study, and may have contributed to the large variation in the stiffness values reported in some prior publications.[17,18,26,35–42] For instance, for photo-crosslinked PEGDA hydrogels with a molecular weight of 3.4 kDa and a pre-polymerization monomer concentration of 20 wt%, the reported shear moduli differ across over an order of magnitude, with values ranging from 13.8 to 502.6 kPa.[26,35–37,39,42] To avoid these problems, we recommend performing in-house quality checks of all commercial PEGDA sources before hydrogel synthesis, especially in cases where reliable physical properties are required.

For each M_n, we fabricated multiple specimens with varying values of initial concentration c_0 above the critical overlap concentration in the PEGDA precursor solution (c^*) (Fig. 4 and Table S2). Within each group, at least five formulations with varied c_0 were studied, including six formulations for PEGDA 0.55 kDa and seven formulations for PEGDA 2.03 kDa and 3.37 kDa due to their common usage and wide commercial availability. c^* describes the weight/volume concentration at which PEGDA coil spheres start to overlap with each other and is an important physical property that affects network formation during photopolymerization. In this work, c^* values were estimated based on the molecular weight of PEGDA (Supplementary Information §2). When the hydrogel is formed at $c_0 < c^*$, there is an increased likelihood of structural heterogeneity due to the formation of irregular voids in the crosslinked network,[43,44] which can result in undesirable effects such as nonuniform swelling and/or mechanical properties,[16,45–47] as well as reduced macromonomer conversion yield.[46–48] Thus, to ensure reliable control of the hydrogel properties, all samples were prepared in the semidilute region where $c_0 > c^*$, and sample properties were compared as a function of $c_0 - c^*$. For convenience and because c^* is conventionally expressed in such a manner, we report our experimental polymer concentrations in terms of weight/volume instead of volume fraction. If needed, both c_0 and c^* can be converted to corresponding volume fractions by dividing by the polymer density (1.18 g/cm^3[14,18]).

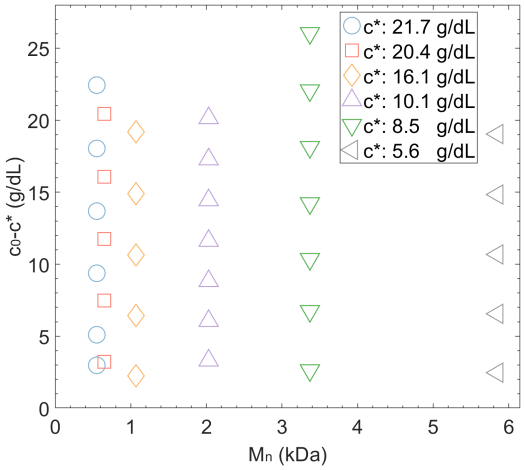

Figure 4: Summary of the synthesis parameters of the PEGDA hydrogels that were examined in this study, showing the values of M_n (from GPC measurement) and c_0 (in the form of $c_0 - c^*$, where c^* is the critical overlap concentration).

We note that the photoinitiator concentration and UV dosing are also important synthesis parameters. However, we found that setting both parameters to high values (4.95 mM LAP and 4 mW/cm^2 for 5 min per side) was advantageous in maximizing the conversion yield of PEGDA acrylate end groups. These settings, when combined with argon purging to reduce the likelihood of oxygen inhibition of polymerization, produced reliable and reproducible material properties across all formulations tested here. Consequently, sol fraction values were measured to be $< 8\%$ for all but one sample set (Table S2 and Supplementary Information §5), indicating that most PEGDA macromonomers have been incorporated in the final materials. It is possible that the combination of high LAP concentration and UV exposure could lead to the generation of reactive oxygen species that could limit some biomedical applications;[49] lower dosage formulations should be explored in that case.

These 35 distinct formulations of hydrogels were synthesized and characterized via uniaxial compression tests. We found remarkable agreement in the mechanical response when comparing replicate measurements of specimens formed using the identical formulations (Fig. S10 to Fig. S15), thanks to the high-precision fabrication technique and processing protocols employed. For each formulation, the G and α parameters were extracted from measurement data via curve fitting to the Yeoh model

presented in Equation 1 (Table S2). Next, we established empirical predictive models for G and α based on analyzing their relationship with M_n and c_0, to enable prediction of sample mechanics from synthesis parameters.

Predictive Model for Shear Modulus G

According to Flory's classic theory on rubber elasticity,[29,50] for homogeneous ideal networks, the shear modulus of an unswollen network (G_R) is given by

$$G_R = \frac{\rho_p RT}{M_c}, \tag{2}$$

where ρ_p is the density of dry polymer network (1.18 g/cm^3 for PEGDA[14,18]), R is the gas constant (8.3145 J $\cdot$ mol^{-1} $\cdot$ K^{-1}), T is the absolute temperature in K, M_c is the average molecular weight between netpoints. For networks formed from end-functional monomers (or in the case of PEGDA, macromonomer chains) without chain-end defects, M_c is usually assumed to be equal to M_n.

The shear modulus of a fully swollen hydrogel G can also be calculated, and is related to that of the unswollen network by a generalized equation

$$G = G_R \cdot A, \tag{3}$$

where A is a function that accounts for the reduction in shear modulus due to equilibrium swelling, and is usually associated with the polymer volume fraction. For example, for an ideal network fully swollen in a good solvent, Flory-Rehner theory predicts $A(\phi) = \phi^{\frac{1}{3}}$,[30] where ϕ is the polymer volume fraction of the equilibrium swollen gel. If one considers the effect of the polymer volume fraction in the preparation state (ϕ_0), for a swollen gel in a good solvent, $A(\phi_0, \phi) = \phi_0^{\frac{5}{12}} \phi^{\frac{7}{12}}$ is typically used.[12]

Unfortunately, for PEGDA-based hydrogels formed by radical polymerization[16,17] possessing a highly heterogeneous network topology, these equations do not provide an accurate estimation of the shear modulus. More recently these classic models have been modified in an attempt to capture more

complex network architectures by introducing a correction factor that accounts for varied junction functionality and chain end defects.[14,22] However, for highly crosslinked PEGDA networks where the junction functionality is presumed to be large and the sol fraction small,[18,19] the corrective term vanishes and these models revert to their original form. Moreover, the expressions of A in current theories require the knowledge of ϕ, the polymer volume fraction of the equilibrium swollen gel, which cannot be accurately estimated for PEGDA hydrogels without experimental testing.[25,27] We aimed to develop a predictive model that accounts for the fundamental structural differences between PEGDA hydrogel networks and ideal networks, and that eliminates the need to include ϕ as an input parameter. To this end, we derived a data-driven methodology that revealed a functional form of A that is based solely on the synthesis parameters M_n and c_0 and accurately describes the stress-stretch data across a wide range of formulations.

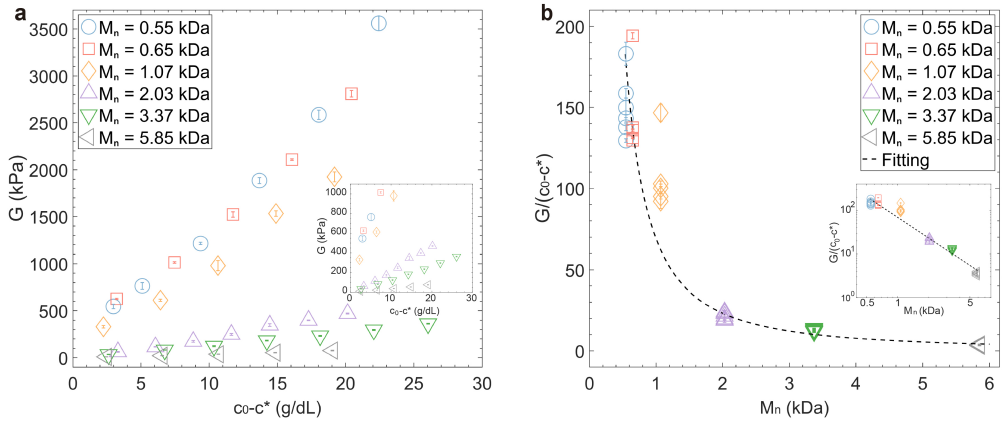

Figure 5: Relationship between the shear modulus G of PEGDA hydrogels and synthesis parameters: (a) measured G versus $c_0 - c^*$. The inset shows the same data in the low-moduli region. (b) G normalized by $c_0 - c^*$ versus M_n, showing multiple curves collapse into one and the corresponding numerical relationship established from weighted fitting. The inset shows the same data plotted in log-log scale.

We first examined the relationship between the experimentally determined shear modulus G and PEGDA concentration, for a range of PEGDA molecular weights (Fig. 5a and Table S2). In all cases, $c_0 > c^*$. Examining the dependency of G on the difference between c_0 and c^* reduces the influence

of the actual value of c^*, which varies with M_n, and provides for a more natural comparison of the hydrogel properties. Qualitatively, a linear dependency between G and $c_0 - c^*$ was observed (Fig. S8), with a slope inversely related to M_n. Based on this observation, we proposed the following relation

$$A = p_1 M_n^{-p_2} (c_0 - c^*), \tag{4}$$

where p_1 and p_2 are fitting parameters. Indeed, when G is normalized by $c_0 - c^*$ and plotted as a function of M_n, we find the data collapse onto one master curve (Fig. 5b), with a few exceptions at low molecular weights and low macromonomer concentrations. Through global weighted fitting across all datasets, we find best fit values of $p_1 = (2.407 \pm 0.990) \times 10^{-6}$ kg $\cdot$ K^{-1} $\cdot$ m^{-3} and $p_2 = 0.576 \pm 0.327$.

Accordingly, the shear modulus can be determined by substitution of Equations 2 and 4 into Equation 3:

$$G = p_1 \frac{\rho_p RT}{M_n^{1+p_2}} (c_0 - c^*). \tag{5}$$

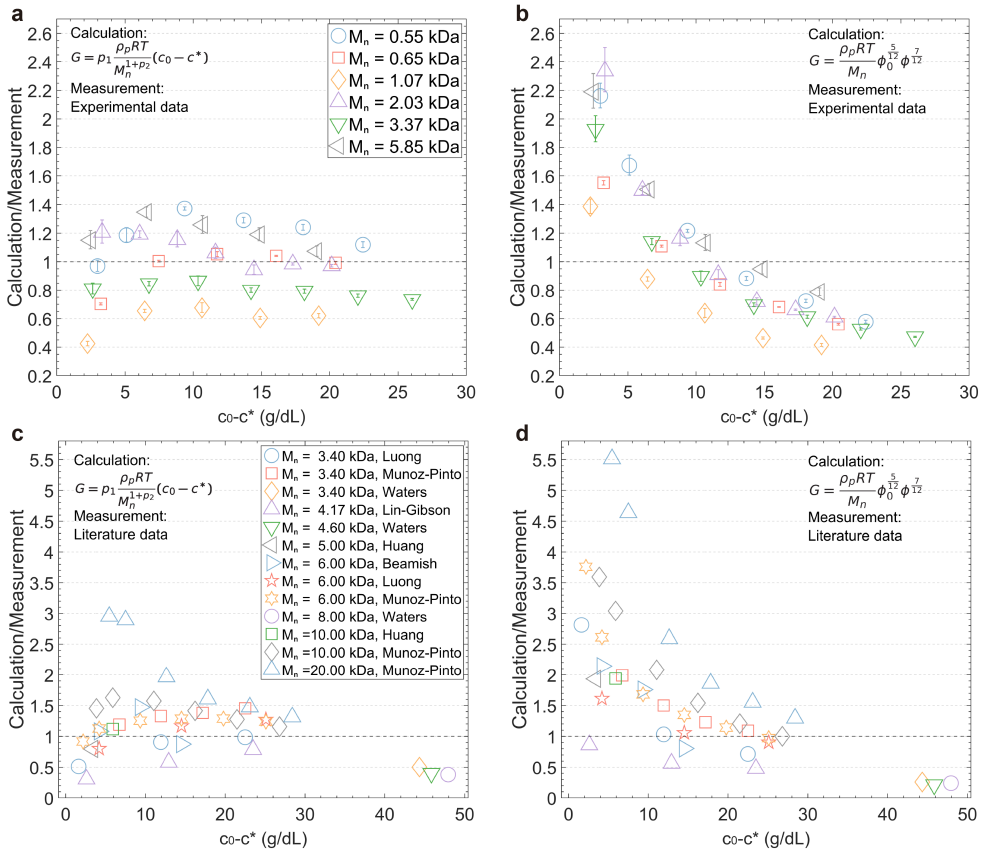

Figure 6: Evaluating the prediction accuracy of the empirical equation developed in this work (Equation 5, where $p_1 = 2.407 \times 10^{-6}$ kg $\cdot$ K^{-1} $\cdot$ m^{-3} and $p_2 = 0.576$) and the classical theory ($G = \frac{\rho_p RT}{M_n}\phi_0^{\frac{5}{12}}\phi^{\frac{7}{12}}$)[12] by comparing the calculated values and measured values of G. (a)–(b): Verifying (a) the empirical equation and (b) the classical theory using experimental data collected in this work. (c)–(d): Verifying (c) the empirical equation and (d) the classical theory using literature data (labeled by the last names of the first authors).

To test the ability of our proposed data-driven model to predict the measured values of G, we compared its accuracy against the classic estimate with ϕ_0 and ϕ values shown in Table S2. To quantify the prediction accuracy, the root-mean-square error and the mean error were evaluated for all datasets (Supplementary Information §8). As demonstrated in Fig. 6 the empirical equation we developed (Equation 5) yields modest prediction errors, with the root-mean-square error (RMSE)

and mean error being 23.5% and 19.4%, respectively. Also, the errors are in general independent of the value of $c_0 - c^*$, and thus could be further reduced by introducing linear correction factors specific to each M_n. This is in contrast to the classical prediction using $G = \frac{\rho_p RT}{M_n}\phi_0^{\frac{5}{12}}\phi^{\frac{7}{12}}$ [12] whereby the prediction errors were substantially larger (with RMSE and mean error being 52.1% and 41.5%, respectively). More importantly, a strong dependence on $c_0 - c^*$ (Fig. 6b) was observed. This leads to significantly larger discrepancies, on the order of 3-fold differences between the measured and predicted values, for formulations where $c_0 \approx c^*$ or $c_0 \gg c^*$. A complementary representation of these differences are provided in Fig. S9, where both equations are plotted with measurement data.

To further test the predictive value of our approach, we validated our model, which was developed using only our own experimental data, against 39 datasets previously published in the literature. We found that our empirical prediction still offers much higher accuracy (RMSE 58.6%, mean error 42.6%) for PEGDA hydrogels with M_n up to 20 kDa, which is outside of the range found in our initial training dataset (Fig. 6c), as compared to the predictions offered from classical theory (RMSE 135.3%, mean error 91.1%, 6d). The agreement between the measurement data and the calculated values based on the new equation is notable, given the substantial differences in hydrogel synthesis (including PEGDA purity, PDI, initiator concentration, illumination conditions, and presence of oxygen) and the mechanical characterization parameters (including compression rate, the use of lubrication, and the degree of swelling of the tested sample) as compared to those of the training dataset.

Predictive Model for Strain-Stiffening Coefficient α

We undertook a similar approach to develop a data-driven model that would capture the full nonlinear material response, including an accurate estimate of the strain-stiffening coefficient α. The measured α values of all samples are shown in Fig. S4 and Table S2. We found that α remained nearly constant for all $M_n = 3.37$ kDa and 5.85 kDa samples, as well as low-concentration $M_n = 2.03$ kDa samples, while the value dropped at high concentrations for other samples. We hypothesize that this decrease in α is an artifact attributed to our inability to sufficiently compress samples

with high stiffness before the force limit was reached (and the measurement terminated), or due to the rupture of brittle samples within or near the elastic limit. This interpretation is supported by the observation that α increased monotonically with the degree of strain stiffening and the final compressive strain, and eventually reached a plateau value after a threshold degree of compression (Fig. S6a and S6b).

Together, these findings suggest that only those samples with sufficient compression or that were compressed to failure even without exhibiting significant strain stiffening can provide an accurate determination of α. For the latter scenario, the individual α values were compiled in Table S2. For the former case, we selectively analyzed the samples whose α values are in the plateau regions when compared to the degree of stiffening and the final compressive strain (Fig. S6a and S6b), as these samples were considered sufficiently compressed and exhibited significant stiffening (Supplementary Information §9). As expected, the datasets selected under this criteria tended to be softer and less brittle samples with higher M_n (Fig. 7a), and thus more likely to be highly compressed before rupture or before the force limit is reached. In this limit, the α values are nearly independent of concentration above c^*.

From the selected datasets, we observed a linear relationship between α and $\frac{1}{M_n}$ (Fig. 7b). Accordingly, we proposed the relation

$$\alpha = \frac{p_3}{M_n}, \tag{6}$$

where p_3 is a fitting parameter. A fit to the data revealed that $p_3 = 1.309 \pm 0.097$ kg $\cdot$ mol^{-1}.

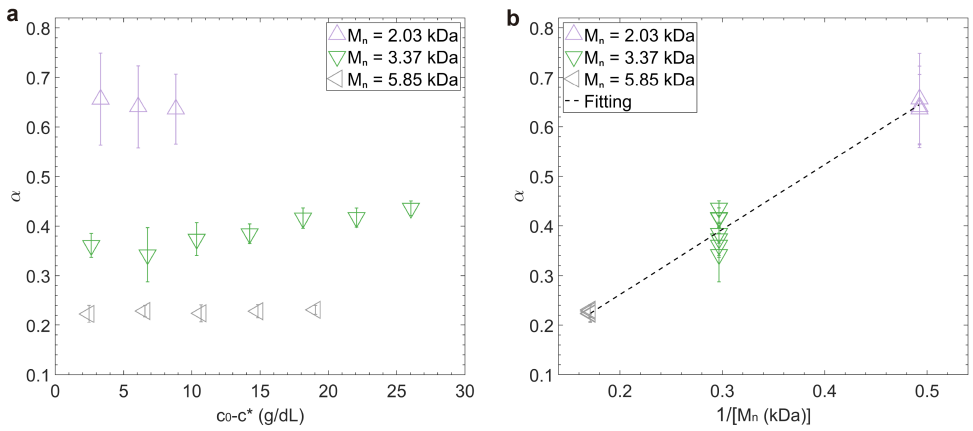

Figure 7: (a) Measured α values of hydrogel samples that were sufficiently compressed (see Supplemental Information §9 for full details); (b) Numerical relationship between these α values and $\frac{1}{M_n}$ according to Equation 6.

As illustrated in Fig. 8, establishing the predictive models for G and α enables the accurate and easy prediction of the full mechanical response for PEGDA hydrogels under uniaxial compression across a wide range of strains, using only two synthesis parameters, M_n and c_0. This is achieved by simple substitution of the empirically determined equations for G (Eq. 5) and α (Eq. 6) into Eq. 1. Comparisons for the full range of formulations are included in the Supplemental Information (Fig. S10 to S15).

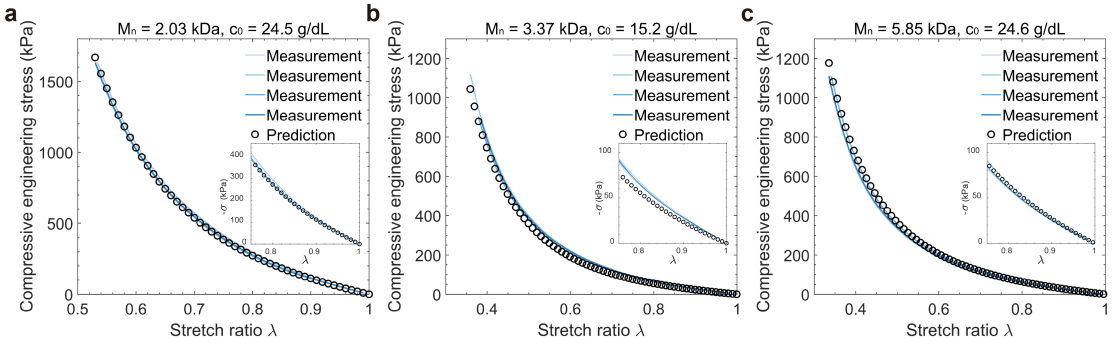

Figure 8: Measured and predicted σ vs. λ curves for PEGDA hydrogels formed with (a) $M_n = 2.03$ kDa, $c_0 = 24.5$ g/dL; (b) $M_n = 3.37$ kDa, $c_0 = 15.2$ g/dL; and (c) $M_n = 5.85$ kDa, $c_0 = 24.6$ g/dL. The insets show zoomed-in views of the curves in the low-strain (high-stretch) region. Note that the measurement curves are in excellent agreement and the individual curves often overlap. The compression endpoint (i.e. smallest values of λ) varies due to samples rupturing at different stretch ratios. Only samples that experienced sufficient compression were included in this analysis (see Supplemental Information §9 for full details). Three exemplar formulations are shown here; the full datasets are available in the Supplemental Information as Figures S9–S14.

Discussion

This work establishes an empirical model to predict the mechanical properties of PEGDA hydrogels using only easily accessible synthesis parameters. To achieve this, we presented a reliable protocol for hydrogel fabrication and characterization that ensured highly reproducible experimental results over a broad range of formulations. To establish the model, we modified the classical theory for G to incorporate the unique features of PEGDA gels observed in experiments. The concentration-related scaling term was found to be proportional to $(c_0 - c^*)$, in contrast to existing theories that scale with the macromonomer concentrations in the preparation state ϕ_0 and in the equilibrium swelling state ϕ. This is corroborated by the fact that the prediction error between classic theory and measured values of G increased significantly for low-molecular-weight samples formed at c_0 close to c^*, and likely reflects the intrinsic structural heterogeneity of PEGDA networks. Although the polymer concentration in the swollen state is not explicitly included in our empirical equation, we found a nearly linear relationship between ϕ and c_0 (Fig. S16), which suggests that the information

contained in ϕ is encoded in c_0.

When tested using both experimental data collected in this study, as well as data previously published in the literature, the empirical equation for G was found to offer much higher prediction accuracy than the classical theory. For the experimental data generated using our robust synthesis and characterization protocols, we find an RMSE of 23.5 % for all formulations. We anticipate that the mechanical properties of PEGDA materials with high PDI values (> 1.4) may deviate from those of samples formed from PEGDA macromonomers with the same M_n but with a narrower molecular weight distribution. It is possible that the prediction error could be reduced by providing a scaling factor that depends on M_n or by fine-tuning the exponent of $(c_0 - c^*)$. For simplicity and generalizability, these were not attempted in this study. Despite these simplifications, it is clear that our framework provides guidance in selecting preparation parameters that can access targeted elastic properties. For example, we can tune the shear modulus G at a constant polymer concentration by varying the molecular weight of the macromonomer (see Table S3, Data Group 1), or can achieve similar values of G through differing combinations of M_n and c_0 (see Table S3, Data Group 2)

Our empirically derived expression for α demonstrates that for samples experiencing significant compression, the extent of strain stiffening does not depend on polymer concentration, and is inversely proportional to M_n which provides a measure of the length of the PEG chains. We anticipate the PEG chains form important crosslinking segments between polyacrylate backbones within the heterogeneous network. Our results indicate that shorter PEG chains provide a stronger response, and that the polyacrylate chains play a minor role in stiffening.

With this framework, we demonstrated an accurate prediction of the full stress vs. stretch ratio response under compression for a large set of formulations and specimens. The use of the Yeoh model is advantageous for applications where the PEGDA network would likely undergo a high degree of deformation, for example in engineered tissues near moving parts such as joints, in soft robotics applications, or for compression-triggered delivery systems. We anticipate that this general form of the presented predictive framework could also be applied to other telechelic or end-linked

hydrogel networks such as poly(ethylene) glycol dimethacrylate. This study creates the groundwork for the further development of analytical microscale models of such networks, while providing key correlations between preparation conditions and mechanical response that enable rational, phenomenological material design.[20,28]

Conclusions

A framework to understand and predict the mechanical properties of structurally heterogeneous, fully swollen PEGDA hydrogels formed in the semidilute regime was developed. Using highly reproducible synthesis and measurement protocols, 35 formulations of PEGDA hydrogels were fabricated and characterized. Using a two-term Yeoh hyperelastic model that incorporates the elastic shear modulus G and compressive strain-stiffening parameter α, we demonstrated that the mechanical response under uniaxial compression could be precisely predicted through knowledge of only two synthesis parameters, M_n and c_0. This simple data-driven framework enables the rational design of PEGDA hydrogels with tailored mechanical properties before any experiments are conducted, extending the capabilities of what can be achieved using current polymer theories.

Supporting Information

The Supporting Information is available free of charge at https://pubs.acs.org/doi/10.1021/acsbiomaterials.x.

Additional experimental data including results from gel permeation chromatography, swelling studies, and a video of a representative compression test; additional details of the mold fabrication, glass treatment, and mechanical measurements; additional details of the estimation of the critical overlap concentration and error analysis; additional ‘discussion of the strain stiffening response at high polymer concentrations; additional details including photographs of the hydrogel materials during compression; additional data including graphical comparisons of the measured and predicted values of modulus and stress; additional details summarizing the composition and measurement results of the study.

Acknowledgments

This research was primarily supported by a grant United States National Science Foundation (NSF, Award No. DMR-2004937) and the United States–Israel Binational Science Foundation (BSF, Award No. 2019742), Jerusalem, Israel. Partial support was provided by the MRSEC Program of the NSF under Award No. DMR-2308708 and the DMREF program of the NSF under Award No. DMR-2118497. M.L. is a fellow of the Ariane de Rothschild Women Doctoral Program. This work made use of experimental facilities provided by BioPACIFIC Materials Innovation Platform of the National Science Foundation under Award No. DMR-1933487 and the MRSEC Program of the NSF under Award No. DMR-2308708; a member of the NSF-funded Materials Research Facilities Network (www.mrfn.org).

References

(1) Durst, C. A.; Cuchiara, M. P.; Mansfield, E. G.; West, J. L.; Grande-Allen, K. J. *Acta Biomater.* **2011**, *7*, 2467–2476.

(2) Soman, P.; Chung, P. H.; Zhang, A. P.; Chen, S. *Biotechnol. Bioeng.* **2013**, *110*, 3038–3047.

(3) Leslie-Barbick, J. E.; Moon, J. J.; West, J. L. *J. Biomater. Sci. Polym. Ed.* **2009**, *20*, 1763–1779.

(4) Burdick, J. A.; Anseth, K. S. *Biomaterials* **2002**, *23*, 4315–4323.

(5) Vehse, M.; Petersen, S.; Sternberg, K.; Schmitz, K.-P.; Seitz, H. *Macromol. Symp.* **2014**, *346*, 43–47.

(6) McAvoy, K.; Jones, D.; Thakur, R. R. S. *Pharm. Res.* **2018**, *35*, 36.

(7) Xue, P.; Zhang, X.; Chuah, Y. J.; Wu, Y.; Kang, Y. *RSC Adv.* **2015**, *5*, 75204–75209.

(8) Kaytanlı, B.; Khankhel, A. H.; Cohen, N.; Valentine, M. T. *Soft Matter* **2020**, *16*, 4192–4199.

(9) Aramesh, M.; Mergenthal, S.; Issler, M.; Plochberger, B.; Weber, F.; Qin, X.-H.; Liska, R.; Duda, G. N.; Huppa, J. B.; Ries, J.; Schütz, G. J.; Klotzsch, E. *Nano Lett.* **2021**, *21*, 507–514.

(10) Decock, J.; Schlenk, M.; Salmon, J.-B. *Lab Chip* **2018**, *18*, 1075–1083.

(11) Rogers, C. I.; Oxborrow, J. B.; Anderson, R. R.; Tsai, L.-F.; Nordin, G. P.; Woolley, A. T. *Sens. Actuators B Chem.* **2014**, *191*.

(12) Obukhov, S. P.; Rubinstein, M.; Colby, R. H. *Macromolecules* **1994**, *27*, 3191–3198.

(13) Anseth, K. S.; Bowman, C. N.; Brannon-Peppas, L. *Biomaterials* **1996**, *17*, 1647–1657.

(14) Richbourg, N. R.; Wancura, M.; Gilchrist, A. E.; Toubbeh, S.; Harley, B. A. C.; Cosgriff-Hernandez, E.; Peppas, N. A. *Science Advances* **2021**, *7*, eabe3245.

(15) Katashima, T.; Asai, M.; Urayama, K.; Chung, U.-I.; Sakai, T. *J. Chem. Phys.* **2014**, *140*, 074902.

(16) Malo de Molina, P.; Lad, S.; Helgeson, M. E. *Macromolecules* **2015**, *48*, 5402–5411.

(17) Waters, D. J.; Engberg, K.; Parke-Houben, R.; Hartmann, L.; Ta, C. N.; Toney, M. F.; Frank, C. W. *Macromolecules* **2010**, *43*, 6861–6870.

(18) Beamish, J. A.; Zhu, J.; Kottke-Marchant, K.; Marchant, R. E. *J. Biomed. Mater. Res. A* **2010**, *92*, 441–450.

(19) Peters, R.; Litvinov, V. M.; Steeman, P.; Dias, A. A.; Mengerink, Y.; van Benthem, R.; de Koster, C. G.; van der Wal, S.; Schoenmakers, P. *J. Chromatogr. A* **2007**, *1156*, 111–123.

(20) Richbourg, N.; Wechsler, M. E.; Rodriguez-Cruz, J. J.; Peppas, N. A. *Nature Reviews Bioengineering* **2024**, 1–13.

(21) Richbourg, N. R.; Peppas, N. A. *Progress in Polymer Science* **2020**, *105*, 101243.

(22) Richbourg, N. R.; Peppas, N. A. *Biomaterials* **2023**, *301*, 122272.

(23) Cohen, N.; McMeeking, R. M. *Journal of the Mechanics and Physics of Solids* **2019**, *125*, 666–680.

(24) Cohen, N.; Du, C.; Wu, Z. L. *Macromolecules* **2021**, 10.1021/acs.macromol.1c01927.

(25) Jimenez-Vergara, A. C.; Lewis, J.; Hahn, M. S.; Munoz-Pinto, D. J. *Journal of Biomedical Materials Research Part B: Applied Biomaterials* **2018**, *106*, 1339–1348.

(26) Cha, C.; Jeong, J. H.; Shim, J.; Kong, H. *Acta Biomater.* **2011**, *7*, 3719–3728.

(27) Padmavathi, N. C.; Chatterji, P. R. *Macromolecules* **1996**, *29*, 1976–1979.

(28) Levin, M.; Tang, Y.; Eisenbach, C. D.; Valentine, M. T.; Cohen, N. *Macromolecules* **2024**, *57*, 7074–7086.

(29) Flory, P. J., *Principles of polymer chemistry*; Cornell University Press: Ithaca, N.Y., 1953.

(30) Flory, P. J.; Rehner, J. *J. Chem. Phys.* **1943**, *11*, 521–526.

(31) Simič, R.; Mandal, J.; Zhang, K.; Spencer, N. D. *Soft Matter* **2021**, *17*, 6394–6403.

(32) Fairbanks, B. D.; Schwartz, M. P.; Bowman, C. N.; Anseth, K. S. *Biomaterials* **2009**, *30*, 6702–6707.

(33) Yeoh, O. H. *Rubber Chem. Technol.* **1993**, *66*, 754–771.

(34) Ogden, R. W., *Non-linear Elastic Deformations*; Courier Corporation: 1997.

(35) Rennerfeldt, D. A.; Renth, A. N.; Talata, Z.; Gehrke, S. H.; Detamore, M. S. *Biomaterials* **2013**, *34*, 8241–8257.

(36) Luong, P. T.; Browning, M. B.; Bixler, R. S.; Cosgriff-Hernandez, E. *J. Biomed. Mater. Res. A* **2014**, *102*, 3066–3076.

(37) Munoz-Pinto, D. J.; Samavedi, S.; Grigoryan, B.; Hahn, M. S. *Polymer* **2015**, *77*, 227–238.

(38) Lin-Gibson, S.; Jones, R. L.; Washburn, N. R.; Horkay, F. *Macromolecules* **2005**, *38*, 2897–2902.

(39) Della Sala, F.; Biondi, M.; Guarnieri, D.; Borzacchiello, A.; Ambrosio, L.; Mayol, L. *J. Mech. Behav. Biomed. Mater.* **2020**, *110*, 103885.

(40) Huang, Y.; Jayathilaka, P. B.; Islam, M. S.; Tanaka, C. B.; Silberstein, M. N.; Kilian, K. A.; Kruzic, J. J. *Acta Biomater.* **2022**, *138*, 301–312.

(41) Zhang, H.; Wang, L.; Song, L.; Niu, G.; Cao, H.; Wang, G.; Yang, H.; Zhu, S. *J. Appl. Polym. Sci.* **2011**, *121*, 531–540.

(42) Browning, M. B.; Cosgriff-Hernandez, E. *Biomacromolecules* **2012**, *13*, 779–786.

(43) Nishi, K.; Asai, H.; Fujii, K.; Han, Y.-S.; Kim, T.-H.; Sakai, T.; Shibayama, M. *Macromolecules* **2014**, *47*, 1801–1809.

(44) Gomes, C.; Dias, R. C. S.; Costa, M. R. P. F. N. *Processes* **2019**, *7*, 237.

(45) Mercado-Montijo, J.; Anstine, D. M.; Rukmani, S. J.; Colina, C. M.; Andrew, J. S. *Soft Matter* **2022**, *18*, 3565–3574.

(46) Liu, W.; Gong, X.; Zhu, Y.; Wang, J.; Ngai, T.; Wu, C. *Macromolecules* **2019**, *52*, 8956–8966.

(47) Sakai, T.; Katashima, T.; Matsushita, T.; Chung, U.-I. *Polym. J.* **2016**, *48*, 629–634.

(48) Orakdogen, N.; Kizilay, M. Y.; Okay, O. *Polymer* **2005**, *46*, 11407–11415.

(49) Rizzo, R.; Petelinšek, N.; Bonato, A.; Zenobi-Wong, M. *Advanced Science* **2023**, *10*, 2205302.

(50) Treloar, L. R. G., *The physics of rubber elasticity*; Oxford University Press, USA: 1975.

A data-driven analytical predictive model for PEGDA hydrogel mechanics based on synthesis parameters only

Experiments

Soft-lithography-based high-precision fabrication ensures highly reproducible data

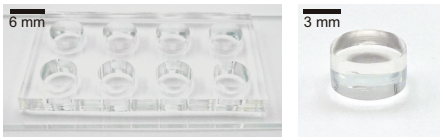

Mechanical property extraction from uniaxial compression tests

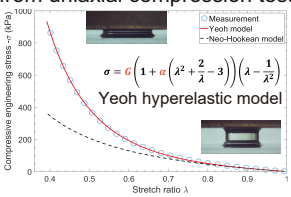

Data-driven model development

Synthesis parameters

- Molecular weight (Mn)
- Initial concentration ($c_0 > c^*$)

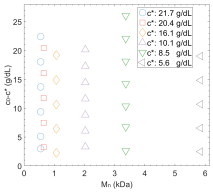

Analysis of 35 sets of data

Mechanical parameters

Shear modulus (G) Strain-stiffening coefficient (α)

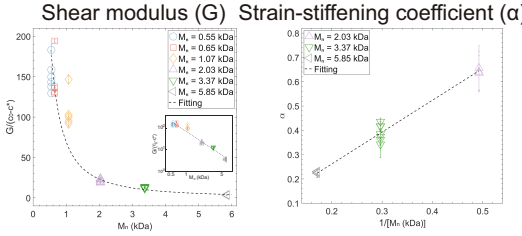

Key results

A simple & effective model to guide rational material design over full range of compression

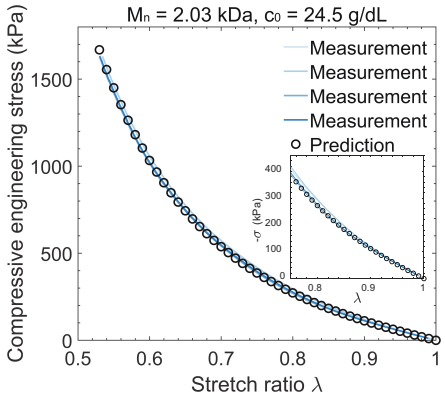

TOC Graphic